Acta Biomaterialia 21 (2015) 132–141

Contents lists available at ScienceDirect

Acta Biomaterialia

journal homepage: www.elsevier.com/locate/actabiomat

Multidimensional characterisation of biomechanical structures by combining Atomic Force Microscopy and Focused Ion Beam: A study of the rat whisker

Vahid Reza Adineh [a], Boyin Liu [a], Ramesh Rajan [b], Wenyi Yan [a], Jing Fu [a,*]

[a] Department of Mechanical and Aerospace Engineering, Monash University, Clayton, VIC 3800, Australia
[b] Department of Physiology, Monash University, Clayton, VIC 3800, Australia

ARTICLE INFO

Article history:
Received 12 September 2014
Received in revised form 23 March 2015
Accepted 23 March 2015
Available online 31 March 2015

Keywords:
Rat whisker
Biomechanics
Atomic Force Microscopy
Focused Ion Beam
Elastic modulus

ABSTRACT

Understanding the heterogeneity of biological structures, particularly at the micro/nano scale can offer insights valuable for multidisciplinary research in tissue engineering and biomimicry designs. Here we propose to combine nanocharacterisation tools, particularly Focused Ion Beam (FIB) and Atomic Force Microscopy (AFM) for three dimensional mapping of mechanical modulus and chemical signatures. The prototype platform is applied to image and investigate the fundamental mechanics of the rat face whiskers, a high-acuity sensor used to gain detailed information about the world. Grazing angle FIB milling was first applied to expose the interior cross section of the rat whisker sample, followed by a "lift-out" method to retrieve and position the target sample for further analyses. AFM force spectroscopy measurements revealed a non-uniform pattern of elastic modulus across the cross section, with a range from 0.8 GPa to 13.5 GPa. The highest elastic modulus was found at the outer cuticle region of the whisker, and values gradually decreased towards the interior cortex and medulla regions. Elemental mapping with EDS confirmed that the interior of the rat whisker is dominated by C, O, N, S, Cl and K, with a significant change of elemental distribution close to the exterior cuticle region. Based on these data, a novel comprehensive three dimensional (3D) elastic modulus model was constructed, and stress distributions under realistic conditions were investigated with Finite Element Analysis (FEA). The simulations could well account for the passive whisker deflections, with calculated resonant frequency as well as force–deflection for the whiskers being in good agreement with reported experimental data. Limitations and further applications are discussed for the proposed FIB/AFM approach, which holds good promise as a unique platform to gain insights on various heterogeneous biomaterials and biomechanical systems.

1. Introduction

Sensory information is actively acquired by animals such as rats with their whiskers (vibrissae) playing an essential role in sensing. These tactile detectors are actively moved through the environment, in a process known as whisking, to sense position, shape, size, and surface features of objects [1–5] which are then fed to neurons to the brain. Sensory information gained from contact of the tip or the upper part of the whisker with an object is transmitted to neurons located at the whisker base and is therefore likely to be governed by the whisker's mechanical and chemical properties. Understanding the biomechanics of the rat whisker system is critical in understanding the message that is fed to the neurons for decoding by the brain and can also help in designing robust robotic active sensing and exploratory systems. Unsurprisingly, the whiskers have therefore been the subject of many analytic and integrated studies including simulation, modelling, chemical and mechanical approaches to study anatomical and physiological properties of real whiskers and designing artificial whiskers [6–29]. However, one limitation in the biomechanics studies is that the whiskers have been assumed to be homogeneous, as conventional mechanical measurements were technologically restricted from accessing and measuring the interiors of the whisker. The diameter of a typical rat whisker is of tens of micrometres, and uniaxial tensile tests [22] of single whiskers *ex vivo* have been performed to determine its elastic modulus. Recently, nanoindentation on the whisker surface was used to obtain a more accurate value for the modulus *in situ*, which was then assumed to be the "universal" modulus of a whisker [13,15]. The presumption of structural homogeneity of a whisker is challenged by optical imaging investigations showing the whiskers have an anisotropic

* Corresponding author.
E-mail address: jing.fu@monash.edu (J. Fu).

http://dx.doi.org/10.1016/j.actbio.2015.03.028
1742-7061/

cross-sectional structure with clear layers and hollow regions being visible [28]. The challenge to bridge the modulus measurements with resonance frequencies results [21] also implies that more knowledge is required by exploring the structural and mechanics of the whisker interior to further understand this intricate sensory system.

Atomic Force Microscopy (AFM) provides an *in situ* approach to probe the mechanical properties of objects; here, sharp cantilever tips are indented into the sample surface, and the elastic modulus is derived from a force–deflection curve. By selecting different tips, this force spectroscopy technique has been successfully applied to characterise soft cells and tissues, to explore their mechanics at nanometre resolution [30–32]. One limitation, however, is that AFM investigations are only confined to the top nanoscale layer of the sample, and leave a wealth of important information beneath the probed regions. Another nanoengineering tool, Focused Ion Beam (FIB), has proven to be superior to a conventional microtome to "slice" biological samples with regard to precision and compression artefacts [33,34]. It also allows the imaging of cell-material interfaces previously inaccessible [35,36], and of cellular interiors by combining different chemical imaging methods such as Secondary Ion Mass Spectrometry (SIMS) [37], Atom Probe Tomography (APT) [38] and synchrotron X-ray [39]. In a previous study combining FIB and AFM, porous polymer surfaces were prepared by FIB milling to achieve the required flatness, and AFM was employed to obtain the surface morphology but investigation of the mechanics was not performed [40].

In the current study, we first developed an integrated novel approach combining FIB and AFM force spectrometry to probe the elastic modulus of the interior of biological samples. Using the relatively new AFM mode of PeakForce Quantitative Nanomechanical Property Mapping (PFQNM), which provided high spatial resolution nanomechanical information, we found and quantified a non-uniform distribution of modulus across the interior section of the rat whisker. Chemical mapping of the same rat whisker cross section was done using Energy-dispersive X-ray spectroscopy (EDS). The second objective was to explore the structural mechanics of the rat whisker, and to build a 3D biomechanical model of this high-acuity tactile sensor. For this, the obtained elastic modulus distribution was incorporated into Finite Element Analysis (FEA), and simulation results obtained for stress distribution and frequency for the complete whisker model. A summary of the experiments for mechanical and chemical characterisation of rat whisker interior cross section using FIB, SEM, AFM and EDS is presented in Fig. 1.

2. Materials and methods

2.1. FIB lift-out based whisker cross section (disc) preparation

Rat whisker samples were obtained from an anaesthetised 3-month old (adult) female Sprague–Dawley rat, by grasping the base with a fine forceps and pulling out from the rat's face [15]. For the study of the interior of whisker sample, it is necessary to expose the interior cross sections first for further analysis. To allow for AFM probing of the whisker interior, we developed a protocol similar to FIB lift-out, a common technique for Transmission Electron Microscopy (TEM) sample preparation [41]. A "cut-off" disc shaped subsample can be retrieved from the whisker and positioned on a solid substrate for access by additional probes. All FIB and SEM tasks including milling, lift-out and mounting on silicon substrate were performed on a dual beam SEM-FIB (Helios NanoLab 600i, FEI company, OR, USA).

The morphology of the rat whisker sample is presented in Fig. 2; In Fig. 2a, SEM image of the exterior cuticle is acquired after applying 10 nm of silver coating to minimise the charging effect, and Fig. 2b shows the interior cross section of the rat whisker after being exposed by FIB milling (Ga^+, 30 keV, ion currents > 1 nA). Fig. 2c introduces several regions which can be distinguished in the exposed cross section of the rat whisker including cuticle, cortex, cortex-medulla and medulla. Also shown in Fig. 2c are exterior cuticle, FIB based platinum (Pt) deposition for securing the sample on the substrate and Pt deposition for milling protection during cleaning milling of the interior part.

Due to the complexity of the experiments, several trial-and-error tests were performed to determine the appropriate milling parameters and sample transfer procedure. In the first attempt, an in-SEM micromanipulator (MM3A-EM, Kleindiek Nanotechnik GmbH, Reutlingen, Germany) was used for manipulating the milled whisker cross sections, and two trials are shown in Fig. 3(a1–4) and (b1–4). Disc shaped cross section samples were milled off successfully with FIB, and the samples were transferred to a Si substrate by securing the samples on the micromanipulator tip with FIB based Pt deposition.

One challenge for FIB lift-out is that further manipulation of a disc-shaped sample is non-trivial, particularly for laying down the cross section side on the substrate. In the two attempts shown in Fig. 3a and b, the micromanipulator tip was attached to different locations of the cross section, but the orientations of the samples on the substrate were not easily controlled. Hence a microgripper (MGS2-EM, Kleindiek Nanotechnik GmbH, Reutlingen, Germany)

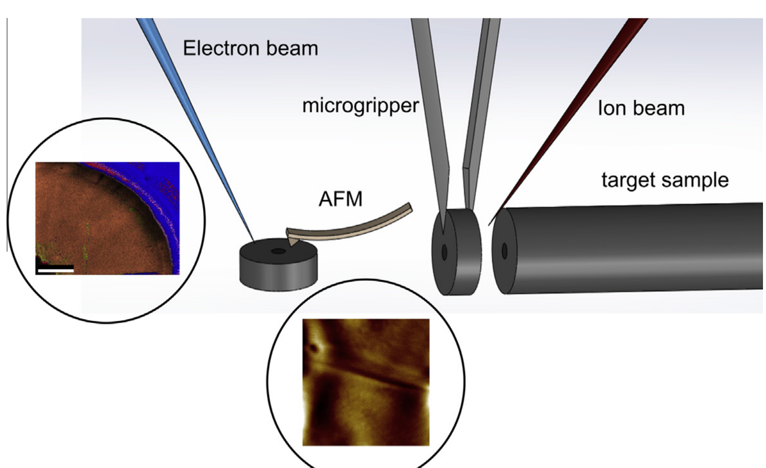

Fig. 1. Schematic diagram of the proposed approach for three dimensional mechanical and chemical characterisation of the rat whisker by combining multiple nanoengineering tools including FIB, SEM, AFM and EDS.

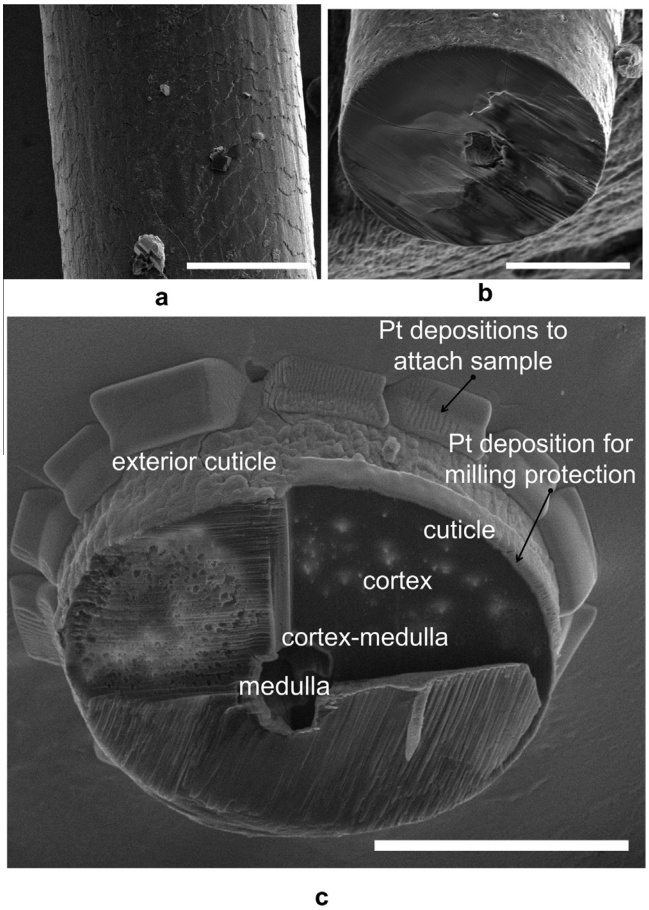

Fig. 2. The anatomy of a rat whisker: (a) the exterior cuticle of the rat whisker imaged by SEM showing scale shape surface morphology, and (b) the cross section of the same whisker exposed by FIB (Ga^+, 30 keV, ion currents > 1 nA) with hollow medulla along the centre axis exposed. (c) SEM image of the retrieved rat whisker cross section positioned on the Si substrate, with labels indicating the inner layers: cuticle, cortex and cortex-medulla. Scale bars: (a): 20 μm, (b): 20 μm and (c): 40 μm.

was employed to transfer the disc sample and to position the sample on the substrate, as demonstrated in Fig. 3c1–4. After two sides of a disc-shaped sample from the whisker were initially milled with FIB (Fig. 3c1), the two jaws of the microgripper were engaged to seize the sample, and then the remainder of the attached part of the disc was milled. After positioning the sample with the flat cross section side on the substrate, Pt was deposited with FIB at the interfaces of the sample and the substrate, to secure the sample (see Fig. 3(c4)). It should be noted that this approach of combining FIB milling, microgripper and platinum deposition has great reproducibility for positioning milled-off biological samples, such as the disc-shaped whisker cross section in this study, for further analysis.

Large current ion beam > 1 nA was applied to mill the sample, producing surface damage such as the curtaining effect visible on the cross section of the whisker sample (Fig. 2c). To minimise such artefacts, additional Pt coating for milling protection was added on the exterior cuticle side of the sample, followed by cleaning milling with FIB parallel to the cross section surface to expose a pristine region of the cross section (upright darker quarter in Fig. 2c). The minimal surface roughness of the pristine region implied that the milling artefacts are negligible with this treatment, and as the ion beam was engaged in grazing angle, damage on the surface was expected to be minimal [42,43].

2.2. AFM 3D topography and modulus calculations

Current reports on various biological systems and materials highlight the unique features of the recently developed PeakForce Quantitative Nanomechanical Property Mapping (PFQNM) mode [44,45] for the study of biological systems [46–49] as well as other materials [50–52]. Hence this AFM method was used for advanced force-distance (FD) curve-based Atomic Force Microscopy, high resolution topography and Young's modulus measurement of the FIB exposed whisker cross sections. All experiments were conducted under ambient conditions with an AFM instrument (Dimension Icon, Veeco, NY, USA) equipped with PFQNM mode. Scan rate of 1 Hz and 512 scanning lines were applied for scanning the desired regions on the surfaces. During acquisition, the peak force set-point was carefully adjusted online using Veeco software (NanoScope version 7.2) to obtain a better fit between trace and retrace signals. Offline analyses were performed with an AFM data processing software package (NanoScope Analysis 1.40, Bruker, Billerica, Massachusetts, USA) based on DMT model [53]. The spring constant and deflection sensitivity of tips were calibrated using the reference sample, and the same AFM probe was used for study of both interior cross section and exterior cuticle. The cantilever spring constants were calibrated using the thermal noise method implemented in the Veeco software (NanoScope version 7.2) and were assumed to have a 5% error [54].

In the PFQNM mode, appropriate probe selection is crucial. As mentioned in the Section 1, the stiffness of the whisker exterior cuticle has been reported in previous studies [7,9,12,13,15,21,22] and the modulus of the rat whisker based on these exterior measurements determined to be in the range of 0.09–7.8 GPa. Hence, a triangular cantilever with nominal frequency of 300 kHz and nominal spring constant of 40 N/m (model RTESPA, Bruker, CA, USA) was used in the AFM measurements [45]. In our study, multiple interior regions containing cortex-medulla, cortex and cuticle (Fig. 2c) were probed according to the proposed interior structural characterisation of the rat whisker by Voges et al. [28]. Also, the exterior cuticle surface was measured to compare with previously published results for this region and with the measurements we obtained from the interior section.

2.3. EDS analysis

The SEM-FIB instrument (FEI Quanta 3D FEG, FEI, OR, USA) equipped with an energy dispersive spectrometer (EDAX, NJ, USA) was employed to determine the elemental composition distribution of the whisker interior cross section and the exterior cuticle. EDS map as well as EDS line scan measurements were performed with an electron beam of accelerating voltage 10 kV and current 4 nA. For the EDX line scan, user-defined line length of 35 μm and 60 μm on the interior section and exterior cuticle were utilised respectively, with a 100 nm spot interval. Analyses were done using EDAX-TEAM software (EDAX, NJ, USA).

2.4. Finite Element Analysis

In previous reports of the whisker modelled as a cantilever beam, it was suggested that the stiffness properties of the whisker might be directly linked to the rat's ability to perform accurate radial distance discrimination [7]. As such, the modulus results we determined from the earlier part of the study were incorporated to build a new three dimensional mechanical model of the rat whisker, followed by simulations using this whisker model under various physiological conditions, e.g. stress distribution across the whisker base with applied load during whisking. As described above, since there are no receptors along the length of the whisker; all sensory information must be mechanically

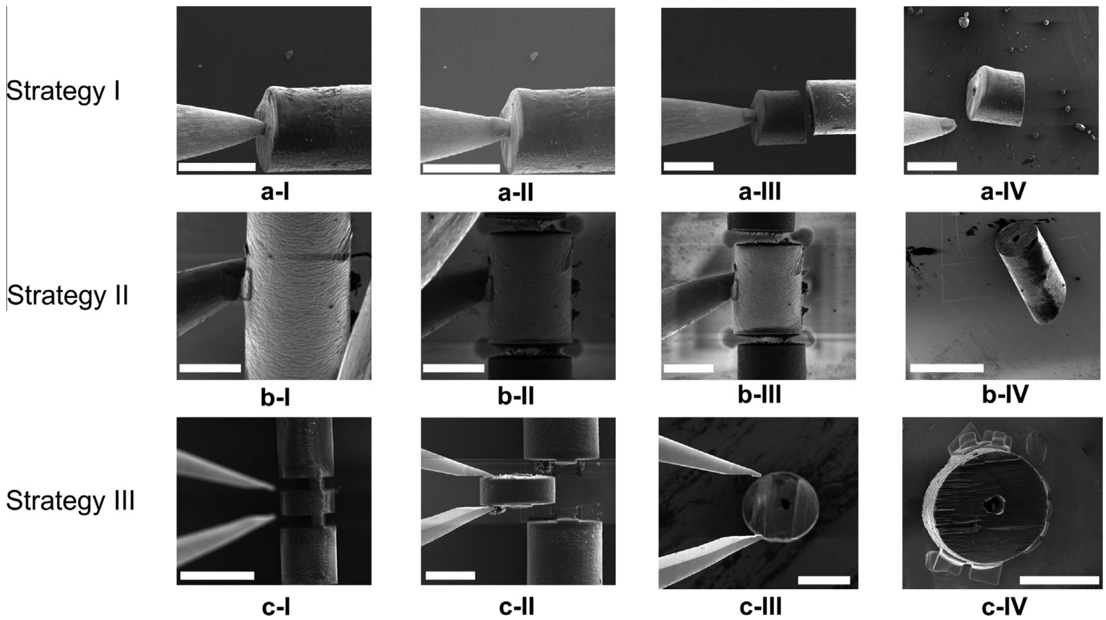

Fig. 3. Strategies to retrieve and position of rat whisker cross sections on the substrate using a micro-manipulator. (a-I)–(a-IV) retrieving the cut-off whisker sample by attaching the micromanipulator needle to the medulla; (b-I)–(b-IV) retrieving the whisker with a micromanipulator attached to the cuticle, with FIB milling performed at the two sides; and with the equipped micro-gripper (c-I)–(c-IV), disc sample of the whisker sample was pinched and positioned on the substrate with expected orientation. Scale bars: a-I to a-IV and b-II, b-III, c-II and c-IV 50 μm; b-I 40 μm; b-IV and c-I 100 μm.

transduced back to receptors as reflected by the stress distribution at the whisker base [7].

Rats typically have rows of five to nine whiskers on each side of their face, and the lengths of these whiskers can be up to 50 mm [55,56]. Diameters of the base and end tip of the rat whiskers vary from 0.085 mm to 0.18 mm and 0.001 mm to 0.035 mm, respectively [21]. In our simulation, a 30 mm long 3D whisker structure was set up, with 50 μm radius at the base and 10 μm at the free end. The detailed internal structures were modelled based on the optical investigations by Voges et al. [28]. During the course of whisking, the free end of the whisker is displaced with applied external force, which is assumed to be normal to the longitudinal axis of the whisker with negligible friction [7]. In the simulation, the actual value of whisking force 1.35×10^{-4} N was extracted from [57] and applied to the tip of the whisker. It should be noted that actual rat whiskers have an inherent curvature, and additional simulations were performed by applying the whisking load to a point close to the whisker base rather than the tip of the whisker to mitigate the influence of curvature [7].

Structural mechanics module of Software package COMSOL Multiphysics (release 4.4, COMSOL Inc., Burlington, MA, USA) was used for all simulations. The models are defined as linear, 3D and under static condition. Each model was meshed with a suggested large number of tetrahedral elements. For simulations of the stress

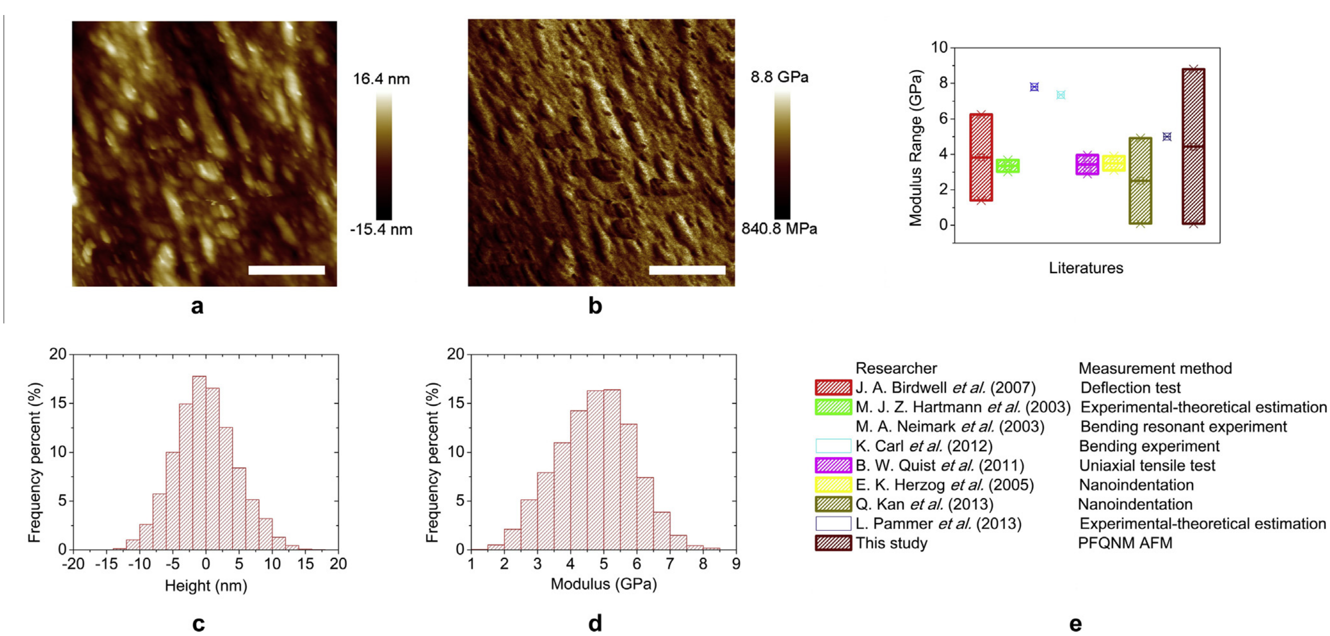

Fig. 4. AFM images of (a) height and (b) modulus measured on the exterior cuticle along with the corresponding histograms (c) and (d). (e) Comparison of the obtained modulus results of the exterior cuticle in this study with those determined by different methods in previous reports. Scale bars: 500 nm.

at the whisker base, fixed constraint boundary condition was considered for the whisker base, while boundary conditions for the other regions were considered as free. The considered load also was applied as a point load to (1) the very end of the whisker tip and (2) 6 mm away from whisker base, and all the stress models were solved using a stationary solver in COMSOL. For simulation of first resonance frequency (FRF), two types of boundary conditions, fixed–fixed and fixed-free, were considered according the experiment setups from Neimark et al. [21]. Fixed constraint boundary condition was applied accordingly, and for all the FRF simulations, the eigenvalue solver of COMSOL was utilised.

3. Results and discussion

3.1. Mechanical characterisation

AFM images of height and stiffness of the whisker exterior cuticle are presented in Fig. 4a and b, along with the corresponding histograms presented in Fig. 4c and d. The figures exhibit microstructures of the surface including elliptic-shaped as well as ridge-like protrusions, with length ranging from 0.2 to 0.5 μm. The stiffness values of these protrusions are also higher than those of the neighbouring areas. In Fig. 4a and c, with pixel size equal to 4 nm, it can be found that the surface height follows a normal distribution with root mean square and average surface roughness of 4.71 nm and 3.77 nm respectively. This implies minimal artefacts between the surface topology and the tip radius. The obtained modulus results show an average value of 4.72 GPa with a standard deviation of 1.16 GPa (Fig. 4b and d). Comparison of the obtained modulus of the exterior surface with those reported in the literature is presented in Fig. 4e [7,9,12,13,15,21,22,57]. The average value in this study is consistent with previous reported values of approximately 4 GPa, while the range is significantly wider.

The agreement with previously published data confirms that the proper type of cantilever was employed for the PFQNM AFM measurements. The wider range can be due to a considerably smaller interaction volume of AFM tip in the PFQNM mode compared to previous methods [44,45]. A larger number of surface microstructures and phases are now distinguishable with the AFM tip in PFQNM mode, and as a result, more detailed distributions of modulus can be determined. Also compared with previous nanoindentation based measurements [13,15], PFQNM mode functions with the same principle as the conventional nanoindentation approach, but elevated frequencies enable a significantly higher data throughput [58].

After exposing the whisker interior with FIB milling, AFM images of adhesion and surface deformation for the cortex-medulla, cortex and cuticle regions of the whisker interior cross section as well as corresponding histograms were recorded and are presented in Fig. 5. The mean values of adhesion for the cortex-medulla, cortex and cuticle parts of the whisker were determined to be 62.3, 84.5, and 49.6 nN respectively (Fig. 5a–c), which highlight the fact that the surface had been sufficiently cleaned by grazing angle FIB milling. In addition, values of surface deformation in all cases are well below the tip radius of 8 nm, suggesting proper selection of cantilever for the measurements (Fig. 5d–f).

Representative distributions of modulus acquired from different regions of the rat whisker interior are presented in Fig. 5g, and distinct patterns for the cortex-medulla, cortex and cuticle regions are shown. For instance, the modulus values for the cortex-medulla region, which is in close proximity to the axis of the whisker, fit a normal distribution. A broader range of modulus values can be found in the cuticle region, possibly due to significant change of material properties towards the exterior surfaces. Indeed, the cuticle part of the whisker shows the highest measured modulus values up to 13.5 GPa which is even higher than the exterior cuticle. These regions of high modulus values are in close proximity to the exterior cuticle, and the mean values for the cortex-medulla, cortex and cuticle parts are 3.65 GPa, 3.79 GPa and 4.79 GPa, respectively. Comparison of elastic modulus values of the three regions indicates that in general, interior regions of the whisker are softer than the exterior cuticle. One exception is that the modulus of cuticle region measured from the cross section is significantly higher compared to the modulus measured on exterior cuticle, suggesting that the stiffness of the cuticle layer is anisotropic. Another interesting observation is that a common significant peak of modulus between 3 and 4 GPa can be found in all the three regions (Fig. 5g), which suggests that the three internal layers may share the same material composition. Together with the topological images (Fig 5a–f), it can be hypothesised that additional nanostructures are also present in cuticle and cortex as revealed by AFM

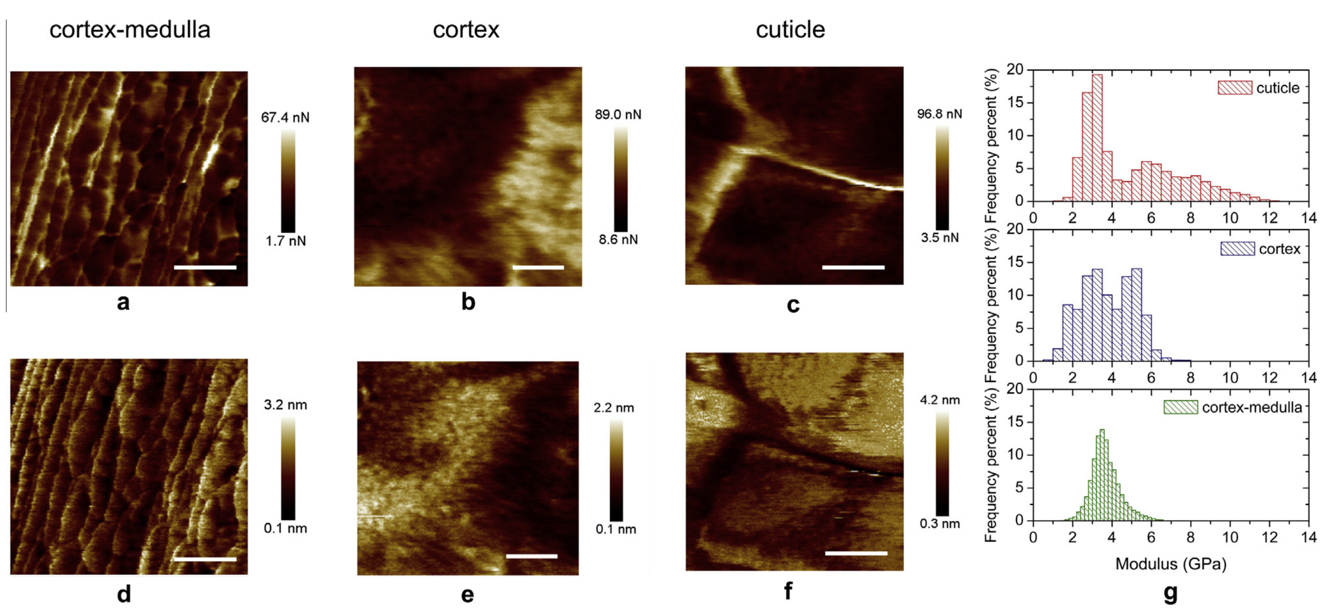

Fig. 5. AFM adhesion images acquired at the different regions on the cross section of the rat whisker: (a) cortex-medulla (b) cortex (c) cuticle, and the corresponding images of surface deformation (d)–(f). Histograms of modulus obtained from those regions (cuticle, cortex and cortex-medulla) are presented in (g). Scale bar: 200 nm.

probing, although a more comprehensive study is required in the future.

3.2. Chemical characterisation

EDS experiments were performed for further investigation of the interior whisker cross sections, and an example of the elemental map obtained through EDS is presented in Fig. 6b. The line scanning along the radius of the interior cross section and the exterior cuticle is highlighted with the dashed lines in Fig. 6a. It can be observed that the interior cross section mostly comprises of C, S, O, N, Cl and K elements. This is also holds for the cuticle except for K which has minimal counts in the cuticle. Other observed elements introduced during sample preparation are gallium from FIB milling, silicon associated to the substrate and platinum that resulted from Pt deposition. As shown in the Fig. 6c and d, these elements are barely found in the interior surface, indicating minimal ion implantation and damage in the final cleaning for AFM measurements. The amounts of C, O and N in the cortex-medulla and cortex regions are slightly higher than those in the cuticle, while for S, the reverse was observed. The distributions of Cl and K are approximately constant through the interior cross section and are less than all of the other elements. No odd behaviour such as significant increase or decrease of elements can be found in the exterior cuticle, while for the interior cross section the one observation is a remarkable decrease of the counts in the cuticle, very close to the exterior cuticle. This is evident by the darker region in the EDS map (see Fig. 6b) of the interior cross section and in the diminishing counts in the EDS line scan across the radius of cross section in Fig. 6e, starting from 32 μm to the exterior cuticle. This fact can be related with the observations of local modulus change, and further correlating chemical imaging with mechanical properties is still an ongoing topic [40,59].

3.3. FEA simulation results

The obtained modulus measurements were incorporated into computer modelling of the whisker, and two different models are considered in the simulations. Fig. 7 presents the cross sections of the modelled internal geometry of the whisker, based upon the model proposed by Voges et al. [28]. According to the report by Voges et al. [28], average share of total diameter is 16% for cuticle, 67–84% for the cortex and 6–15% for the medulla. Depending on the type of whisker, medulla region accounts for 50–75% of the overall length.

In the first model, a uniform modulus value of 4 GPa was applied for all the different internal geometries of the whisker model, similar to the previous reports. For the second model, the Young's modulus of 3.72 GPa; average of AFM measured values of 3.65 GPa and 3.79 GPa for the cortex-medulla and cortex, was applied for the part II of Fig. 7. For the cuticle region (part I), an average modulus value of 4.79 GPa was applied reflecting the actual AFM stiffness measurements at this study. In all of the simulations, Poisson ratio is considered as 0.4 [15] and average density of 1.14 mg/mm^3 [12] was utilised for the whisker. It should be noted that in the non-uniform modulus distribution cases, the

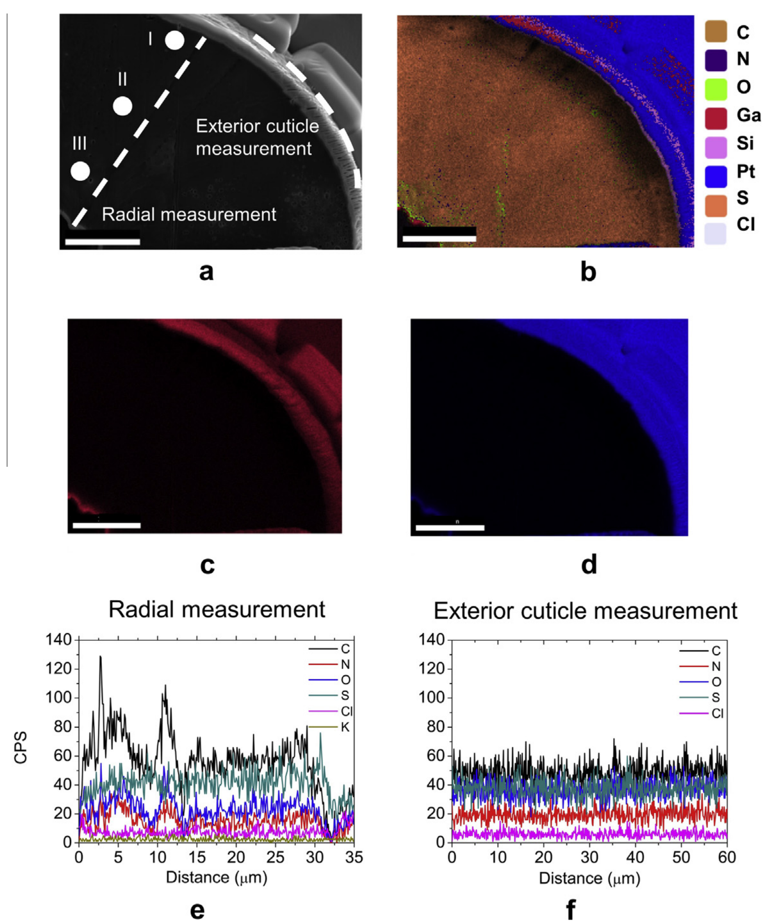

Fig. 6. Energy-dispersive X-ray spectroscopy (EDS) mapping of the interior cross section including the edge of the exterior cuticle. (a) Dashed lines indicate the path of EDS scans in both the interior cross section and the exterior cuticle, while solid circles represent areas sampled for the AFM; (b) Combined EDS maps of the whisker interior cross section; EDS map of (c) Ga and (d) Pt in the interior cross section; (e) Radial measurement – EDS line-scan along the radius of the interior cross section from the cortex-medulla to the cuticle; and (f) Exterior cuticle measurement – EDS line-scan of the exterior cuticle. Scale bars: 10 μm.

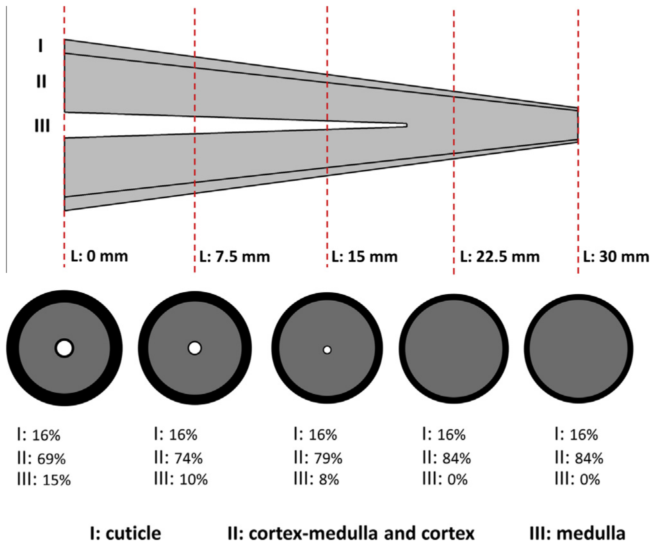

Fig. 7. Schematic of cross sectional views showing the considered interior structure of the mechanical model based upon the proposed structure in Voges et al. [28]. Top image presents the overall model in 2D, with bottom cross sectional views showing percentage contribution of each sublayer along the axis of the whisker.

Poisson's ratio is assumed to be constant for all of the regions due to insufficient data.

To date there is lack of direct experimental measurement of the stresses that occur at the whisker base with different whisking forces applied to the whisker tip or shaft. Several studies provided mechanical properties of rat whiskers including their first resonance frequencies as well as values for whisker deflection subject to the applied forces. Our models in this study were first validated by comparing the experimental observation of rat whisker's FRF [21] and force–deflection measurements [7]. Values of Young modulus, Poisson's ratio, density and geometrical dimensions of considered whiskers are referred to[7,21]. Table 1 presents comparison of simulated FRF of our model for r_{base}/L^2 ratio of 0.55 [10^{-4} mm^{-1}] with the FRF values based on the model proposed by Neimark et al., which is least square fit to experimental measurements [21]. It should be noted that the final simulated values were consistent particularly with the *in vivo* measurements of Neimark et al. [21]. The observed differences, approximately 20%, can be due to the discrepancies of density and modulus values used in the simulation and the actual values that occurred in the experiments [21]. Difference in the geometry such as the considered geometry of the medulla is also possible to affect the final simulation results to some extent.

Further validation included the scenarios in previous experiments by Birdwell et al. [7], while whiskers deflect due to applied horizontal forces imposed at 6 mm from the base. The results were presented in Fig. 8a, and whiskers gamma, E2 and E3 were selected for comparison. The arc length (mm) base diameter (μm) and average modulus (GPa) applied in the simulations were 60.3, 199 and 3.75 for whisker gamma, 48.1, 232 and 1.90 for whisker E2 and 33.3, 189 and 3.9 for whisker E3, respectively. A good agreement between the simulation and experimental results was observed, while some discrepancies occurred with increased force, possibly due to the approximation of end tip diameter and density of whisker. In addition to verifying the integrity of the simulation model, solutions were also tested to be mesh independent and convergent with refining the mesh size. With mesh extension results of the simulated models presented in Fig. 8b, the first principal stress at the whisker base for the uniform and non-uniform structures subject to the applied force are shown to be convergent for each case confirming the stability of the simulation as well as the solutions. It should be noted that the results of these simulations are subject to several constraints. In particular we have ignored several natural whisking factors, such as whisker velocity during whisking, inherent whisker curvature, which are known to be important in natural behaviour.

After model validation, values of principal stress at the whisker base are acquired to assess the effects by whisker deflection. As discussed in the previous sections, stresses in the base follicle are hypothesised to be crucial for object localisation [55], and used to determine surface texture [56,57] and avoid obstacles [58]. Fig. 9a and b present the first principal stress at the whisker base, for both models of uniform and non-uniform modulus distributions. It can be seen that for the same conditions, the amount of produced stresses at the whisker base of the non-uniform modulus model is similar to that in the homogenous model, although slightly higher (~10%) with regard to the maximum stress. The simulations also reveal that regions close to the cuticle experience the highest resultant stresses, as shown in Fig. 9a and b, and this phenomenon extends to the base of the whisker which connects to the follicle.

Also, analysis of Birdwell et al. [7] showed that the error of neglecting the inherent curvature of the whisker can be reasonably decreased provided that the force is imposed at $a/L < 70\%$, where a is the distance from the base and L is the whisker length. Therefore, additional simulations on the considered uniform and non-uniform models were performed and the results are presented in Fig. 9d and e. For these simulations, a larger force of magnitude 1 mN was imposed horizontally at 6 mm from the whisker base, to minimise the effects of inherent curvature of the actual whisker due to large displacement. Results in Fig. 9d and e also confirm similar or modest increase of base stress in the non-homogenous whisker model. Furthermore, resonance is considered to enhance both detection and discrimination of signals in the biological and human-made sensory systems [21]. FRF can also be quantitatively determined with the constructed multi-layer mechanical model with simulated vibration behaviours as shown in Fig 9g–i. For the particular whisker investigated in this study, it is suggested that FRF is in the range of 100 Hz and increases with higher cuticle modulus.

With the proposed AFM/FIB 3D mapping approach and the following simulations, the acquired results can provide a number of insights for developing artificial whisker-based sensory systems. The revealed non-homogenous modulus structures contain a core layer of lower modulus which primarily acts as a "softer" cantilever while the higher moduli regions act as a "stiffer" outer layer. Therefore, minimal forces are needed for large displacements due to the "weaker" core, while at the same time, significant stresses are still present in the whisker base. An improved design of artificial whisker is tested with non-homogenous modulus structure: 16 GPa for the cuticle and same 4 GPa for the cortex-medulla and cortex. The simulated results of artificial whisker were presented in Fig. 9c and f, and the amount of produced stresses at the whisker base increased by approximately 30%.

Table 1
Comparison of FRF values of this study's rat whisker model with r_{base}/L^2 ratio of 0.55 [10^{-4} mm^{-1}] with least square fit to experimental measurements by Neimark et al. [21].

Boundary condition	This study (Hz)	Neimark et al. (*ex vivo*) (Hz)	Neimark et al. (*in vivo*) (Hz)	% difference with Neimark et al. (*ex vivo*)	% difference with Neimark et al. (*in vivo*)
Fixed-free	72	95	90	24	20
Fixed–fixed	141	195	170	27	17

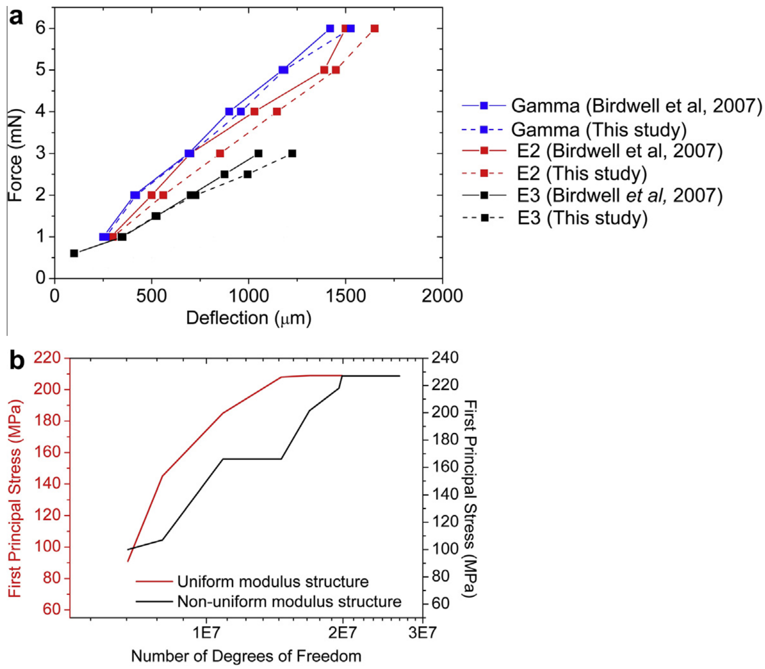

Fig. 8. (a) Comparison of force–deflection graphs simulated in this study with experimental measurements by Birdwell et al. [7] including whiskers Gamma, E2 and E3. (b) Simulated values of first principal stress at the base of the whisker models with increasing mesh size. The actual force was applied to the whisker tip, with both uniform and non-uniform modulus distributions considered.

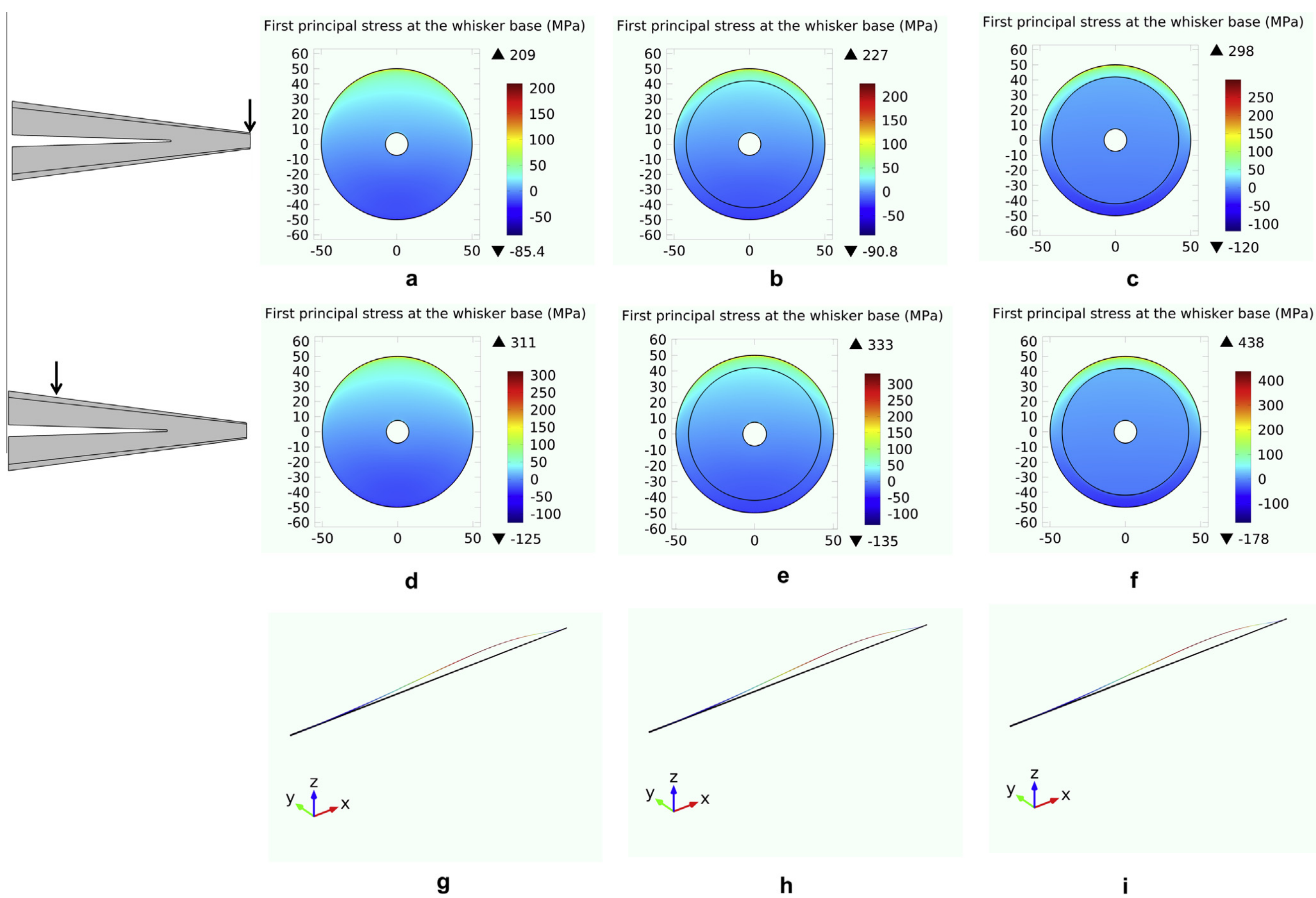

Fig. 9. Mechanical simulation of first principal stress distributions at the whisker base and first resonant frequency (FRF) of the considered whisker models. With forces applied to the whisker tips; cross sectional views of the first principal stress at the whisker base for models of (a) uniform modulus (b) non-uniform modulus and (c) artificial whisker. With forces applied to a location 6 mm from the whisker base, cross sectional views of first principal stress at the whisker base for models of (d) uniform modulus, (e) non-uniform modulus and (f) artificial whisker. In (a)–(f), the unit of the x–y axes is μm and the unit of colour map values is MPa. Simulation of FRF of the whisker based on (g) uniform modulus, (h) non-uniform modulus and (i) artificial whisker, assuming fixed–fixed boundary condition.

Table 2
Comparison of current microanalysis techniques for investigating three dimensional biomechanical systems.

Technique	Resolution/accuracy	Acquisition/imaging	Remarks
X-ray micro/nano tomography	Submicron resolution for laboratory setup, and down to 10 nm resolution based on synchrotron.	Primarily for structure with phase contrast. [60–63]	Fast acquisition, cryo-compatible
Mechanical sectioning (serial block imaging)	~100 nm accuracy in sectioning	Structure (SEM), elemental and molecular mapping feasible by integration with various imaging techniques. [64,65]	Elasticity study infeasible due to mechanical compression
Focused Ion Beam	~10 nm resolution and ~10 nm accuracy in milling	Structure (SEM), elasticity (AFM), elemental and molecular mapping feasible by integration with various imaging techniques. [36,72–74]	Limited sectioning speed, cryo-compatible

4. Conclusions

In this study a prototype platform combining FIB and AFM was developed to investigate mechanical and chemical properties of biomechanical systems using the rat's large face whiskers as a model test system, and both the interior cross section and exterior surface of the rat whisker were investigated. Comparison of current three dimensional microanalysis techniques is summarised in Table 2, which are suitable for small biomechanical systems such as the rat whisker. The recent progress in X-ray imaging particularly and the synchrotron-based systems allow 3D tomography of tissue and single cells towards 10 nm resolution [60–63], but limited information other than density and structure can be revealed. In mechanical sectioning or serial block imaging approach, a microtome is applied to remove thin sections of the sample followed by SEM imaging [64,65]. Potentially chemical imaging can also be integrated to explore the sample in the third dimension after microtoming, but compression of the sample surface is well known and prevents further AFM analysis. FIB milling, as demonstrated in this study, provides high precision surface preparation and sample transfer to enable AFM probing of the sample interior. It should be noted that a trade-off of high resolution is the low material removal rate of FIB, and it will be challenging to explore structures much larger than the rat whisker sample.

To the best of our knowledge, it is the first study providing three dimensional insights of the interior of the rat whisker and a multi-layer mechanical model. "Lift-out" sample preparation followed for AFM probing was performed, and this can be applied in other projects to investigate samples which would otherwise be inaccessible for study. The measured values for the exterior cuticle showed good agreement with previously published results. Non-uniform modulus distribution in the whisker cross section was revealed and quantified, while chemical properties of interior cross section demonstrated similar patterns. Finite element simulations with varied modulus distributions further confirmed that non-uniform modulus distribution of the rat whisker as determined in this study, likely contributes to the high sensitivity of this tactile sensor for natural behaviours although a more comprehensive study is needed. The mechanical and chemical characterisation results can be useful for further developing prototype artificial whiskers [66–69] and for biological study of rat whisker behaviour [1,25–27,70,71]. The characterisation methodologies and protocols developed in this study, although only applied to the rat whisker, can also be extended to studies of a wide range of biomechanical systems in future.

Acknowledgements

This work was performed in part at the Melbourne Centre for Nanofabrication (MCN) in the Victorian Node of the Australian National Fabrication Facility (ANFF). Also, the authors acknowledge use of facilities within the Monash Centre for Electron Microscopy (MCEM). This research used equipment funded by Australian Research Council grant ARC Funding (LE0882821). In addition, the simulation part was supported in part by the Monash e-Research Centre and eSolutions-Research Support Services through the use of the high-memory capability on the Monash Campus HPC Cluster. The authors would like to thank Drs Hemayet Uddin, Fatima Eftekhari, Amelia Liu and Philip Chan for their assistance during this study.

Appendix A. Figures with essential colour discrimination

Certain figures in this article, particularly Figs. 1 and 4–9 are difficult to interpret in black and white. The full colour images can be found in the on-line version, at http://dx.doi.org/10.1016/j.actbio.2015.03.028.

References

[1] Crochet S, Petersen CC. Correlating whisker behavior with membrane potential in barrel cortex of awake mice. Nat Neurosci 2006;9:608–10.
[2] Ferezou I, Haiss F, Gentet LJ, Aronoff R, Weber B, Petersen CC. Spatiotemporal dynamics of cortical sensorimotor integration in behaving mice. Neuron 2007;56:907–23.
[3] Hartmann MJ. Active sensing capabilities of the rat whisker system. Auton Robot 2001;11:249–54.
[4] Lungarella M, Hafner VV, Pfeifer R, Yokoi H. An artificial whisker sensor for robotics. In: IEEE/RSJ International Conference on Intelligent Robots and Systems, 2002. IEEE; 2002. p. 2931–6.
[5] Wolfe J, Hill DN, Pahlavan S, Drew PJ, Kleinfeld D, Feldman DE. Texture coding in the rat whisker system: slip-stick versus differential resonance. PLoS Biol 2008;6:e215.
[6] Berwick J, Johnston D, Jones M, Martindale J, Redgrave P, McLoughlin N, et al. Neurovascular coupling investigated with two-dimensional optical imaging spectroscopy in rat whisker barrel cortex. Eur J Neurosci 2005;22:1655–66.
[7] Birdwell JA, Solomon JH, Thajchayapong M, Taylor MA, Cheely M, Towal RB, et al. Biomechanical models for radial distance determination by the rat vibrissal system. J Neurophysiol 2007;98:2439–55.
[8] Brett-Green BA, Chen-Bee CH, Frostig RD. Comparing the functional representations of central and border whiskers in rat primary somatosensory cortex. J Neurosci 2001;21:9944–54.
[9] Carl K, Hild W, Mampel J, Schilling C, Uhlig R, Witte H. Characterization of statical properties of rat's whisker system. IEEE Sens J 2012;12:340–9.
[10] Carvell GE, Simons DJ. Biometric analyses of vibrissal tactile discrimination in the rat. J Neurosci 1990;10:2638–48.
[11] Chen-Bee CH, Frostig RD. Variability and interhemispheric asymmetry of single-whisker functional representations in rat barrel cortex. J Neurophysiol 1996;76:884–94.
[12] Hartmann MJ, Johnson NJ, Towal RB, Assad C. Mechanical characteristics of rat vibrissae: resonant frequencies and damping in isolated whiskers and in the awake behaving animal. J Neurosci 2003;23:6510–9.
[13] Herzog E, Bahr D, Richards C, Richards R, Rector D. Spatially dependent mechanical properties of rat whiskers for tactile sensing. In: Materials research society symposium proceedings. Cambridge Univ Press; 2005. p. 119.
[14] Ito M. Some quantitative aspects of vibrissa-driven neuronal responses in rat neocortex. J Neurophysiol 1981;46:705–15.
[15] Kan Q, Rajan R, Fu J, Kang G, Yan W. Elastic modulus of rat whiskers–a key biomaterial in the rat whisker sensory system. Mater Res Bull 2013.
[16] Learoyd AE, Lifshitz J. Comparison of rat sensory behavioral tasks to detect somatosensory morbidity after diffuse brain-injury. Behav Brain Res 2012;226:197–204.
[17] Lindauer U, Royl G, Leithner C, Kühl M, Gold L, Gethmann J, et al. No evidence for early decrease in blood oxygenation in rat whisker cortex in response to functional activation. NeuroImage 2001;13:988–1001.

[18] Mégevand P, Troncoso E, Quairiaux C, Muller D, Michel CM, Kiss JZ. Long-term plasticity in mouse sensorimotor circuits after rhythmic whisker stimulation. J Neurosci 2009;29:5326–35.
[19] Millar SE, Miller MW, Stevens ME, Barsh GS. Expression and transgenic studies of the mouse agouti gene provide insight into the mechanisms by which mammalian coat color patterns are generated. Development 1995;121:3223–32.
[20] Minnery BS, Simons DJ. Response properties of whisker-associated trigeminothalamic neurons in rat nucleus principalis. J Neurophysiol 2003;89:40–56.
[21] Neimark MA, Andermann ML, Hopfield JJ, Moore CI. Vibrissa resonance as a transduction mechanism for tactile encoding. J Neurosci 2003;23:6499–509.
[22] Quist BW, Faruqi RA, Hartmann MJ. Variation in Young's modulus along the length of a rat vibrissa. J Biomech 2011;44:2775–81.
[23] Rocamora N, Welker E, Pascual M, Soriano E. Upregulation of BDNF mRNA expression in the barrel cortex of adult mice after sensory stimulation. J Neurosci 1996;16:4411–9.
[24] Yazawa I, Sasaki S, Mochida H, Kamino K, Momose-Sato Y, Sato K. Developmental changes in trial-to-trial variations in whisker barrel responses studied using intrinsic optical imaging: comparison between normal and de-whiskered rats. J Neurophysiol 2001;86:392–401.
[25] Manfredi LR, Saal HP, Brown KJ, Zielinski MC, Dammann JF, Polashock VS, et al. Natural scenes in tactile texture. J Neurophysiol 2014;111:1792–802.
[26] Maravall M, Diamond ME. Algorithms of whisker-mediated touch perception. Curr Opin Neurobiol 2014;25:176–86.
[27] Bagdasarian K, Szwed M, Knutsen PM, Deutsch D, Derdikman D, Pietr M, et al. Pre-neuronal morphological processing of object location by individual whiskers. Nat Neurosci 2013;16:622–31.
[28] Voges D, Carl K, Klauer GJ, Uhlig R, Schilling C, Behn C, et al. Structural characterization of the whisker system of the rat. IEEE Sens J 2012;12:332–9.
[29] Yan W, Kan Q, Kergrene K, Kang G, Feng X-Q. A truncated conical beam model for analysis of the vibration of rat whiskers. J Biomech 2013;46:1987–95.
[30] Thomasy SM, Raghunathan VK, Winkler M, Reilly CM, Sadeli AR, Russell P, et al. Elastic modulus and collagen organization of the rabbit cornea: epithelium to endothelium. Acta Biomater 2014;10:785–91.
[31] Dufrêne YF. Atomic force microscopy, a powerful tool in microbiology. J Bacteriol 2002;184:5205–13.
[32] Plodinec M, Loparic M, Monnier CA, Obermann EC, Zanetti-Dallenbach R, Oertle P, et al. The nanomechanical signature of breast cancer. Nat Nanotechnol 2012;7:757–65.
[33] Marko M, Hsieh C, Schalek R, Frank J, Mannella C. Focused-ion-beam thinning of frozen-hydrated biological specimens for cryo-electron microscopy. Nat Methods 2007;4:215–8.
[34] Heymann JA, Hayles M, Gestmann I, Giannuzzi LA, Lich B, Subramaniam S. Site-specific 3D imaging of cells and tissues with a dual beam microscope. J Struct Biol 2006;155:63–73.
[35] Friedmann A, Hoess A, Cismak A, Heilmann A. Investigation of cell–substrate interactions by focused ion beam preparation and scanning electron microscopy. Acta Biomater 2011;7:2499–507.
[36] Al-Abboodi A, Fu J, Doran PM, Chan PP. Three-dimensional nanocharacterization of porous hydrogel with ion and electron beams. Biotechnol Bioeng 2013;;110:318–26.
[37] Szakal C, Narayan K, Fu J, Lefman J, Subramaniam S. Compositional mapping of the surface and interior of mammalian cells at submicrometer resolution. Anal Chem 2011;83:1207–13.
[38] Narayan K, Prosa TJ, Fu J, Kelly TF, Subramaniam S. Chemical mapping of mammalian cells by atom probe tomography. J Struct Biol 2012;178:98–107.
[39] James SA, Feltis BN, de Jonge MD, Sridhar M, Kimpton JA, Altissimo M, et al. Quantification of ZnO nanoparticle uptake, distribution, and dissolution within individual human macrophages. ACS Nano 2013;7:10621–35.
[40] Virgilio N, Favis BD, Pépin M-F, Desjardins P, L'Espérance G. High contrast imaging of interphases in ternary polymer blends using focused ion beam preparation and atomic force microscopy. Macromolecules 2005;38:2368–75.
[41] Giannuzzi LA, Drown JL, Brown SR, Irwin RB, Stevie FA. Applications of the FIB lift-out technique for TEM specimen preparation. Microsc Res Tech 1998;41:285–90.
[42] Hazekamp J, Doherty S, Elsaesser A, Barnes CA, O'Hagan BMG, McKerr G, et al. Focussed ion beam milling at grazing incidence angles. J Microsc 2011;242:104–10.
[43] Liu B, Uddin H, Ng TW, Paterson DL, Velkov T, Li J, et al. In situ probing the interior of single bacterial cells at nanometer scale. Nanotechnology 2014;25:415101.
[44] Pittenger B, Erina N, Su C. Quantitative mechanical property mapping at the nanoscale with peak force QNM. Bruker application note AN128 2010.
[45] Pittenger B, Erina N, Su C. Mechanical property mapping at the nanoscale using peakforce QNM scanning probe technique. In: Nanomechanical analysis of high performance materials. Springer; 2014. p. 31–51.
[46] Adamcik J, Berquand A, Mezzenga R. Single-step direct measurement of amyloid fibrils stiffness by peak force quantitative nanomechanical atomic force microscopy. Appl Phys Lett 2011;98:193701.
[47] Sweers K, van der Werf K, Bennink M, Subramaniam V. Nanomechanical properties of α-synuclein amyloid fibrils: a comparative study by nanoindentation, harmonic force microscopy, and peakforce QNM. Nanoscale Res Lett 2011;6:1–10.
[48] Wang D, Liang X, Russell TP, Nakajima K. Visualization and quantification of the chemical and physical properties at a diffusion-induced interface using AFM nanomechanical mapping. Macromolecules 2014;47:3761–5.
[49] Sweers KK, van der Werf KO, Bennink ML, Subramaniam V. Atomic force microscopy under controlled conditions reveals structure of C-terminal region of α-synuclein in amyloid fibrils. ACS Nano 2012;6:5952–60.
[50] Zhao B, Song Y, Wang S, Dai B, Zhang L, Dong Y, et al. Mechanical mapping of nanobubbles by peakforce atomic force microscopy. Soft Matter 2013;9:8837–43.
[51] Young T, Monclus M, Burnett T, Broughton W, Ogin S, Smith P. The use of the peakforceTM quantitative nanomechanical mapping AFM-based method for high-resolution Young's modulus measurement of polymers. Meas Sci Technol 2011;22:125703.
[52] Trtik P, Kaufmann J, Volz U. On the use of peak-force tapping atomic force microscopy for quantification of the local elastic modulus in hardened cement paste. Cem Concr Res 2012;42:215–21.
[53] Derjaguin BV, Muller VM, Toporov YP. Effect of contact deformations on the adhesion of particles. J Colloid Interface Sci 1975;53:314–26.
[54] Ohler B. Cantilever spring constant calibration using laser Doppler vibrometry. Rev Sci Instrum 2007;78:063701.
[55] Haidarliu S, Ahissar E. Size gradients of barreloids in the rat thalamus. J Comp Neurol 2001;429:372–87.
[56] Prescott TJ, Pearson MJ, Mitchinson B, Sullivan JCW, Pipe AG. Whisking with robots from rat vibrissae to biomimetic technology for active touch. IEEE Robot Autom Mag 2009;16:42–50.
[57] Pammer L, O'Connor DH, Hires SA, Clack NG, Huber D, Myers EW, et al. The mechanical variables underlying object localization along the axis of the whisker. J Neurosci 2013;33:6726–41.
[58] Sweers K. Nanoscale structural and mechanical properties of alpha-synuclein amyloid fibrils. Universiteit Twente; 2012.
[59] Hughes JJ, Trtik P. Micro-mechanical properties of cement paste measured by depth-sensing nanoindentation: a preliminary correlation of physical properties with phase type. Mater Charact 2004;53:223–31.
[60] Schneider G, Guttmann P, Heim S, Rehbein S, Mueller F, Nagashima K, et al. Three-dimensional cellular ultrastructure resolved by X-ray microscopy. Nat Methods 2010;7:985–7.
[61] Mizutani R, Suzuki Y. X-ray microtomography in biology. Micron 2012;43:104–15.
[62] Yue S, Lee PD, Poologasundarampillai G, Yao Z, Rockett P, Devlin AH, et al. Synchrotron X-ray microtomography for assessment of bone tissue scaffolds. J Mater Sci Mater Med 2010;21:847–53.
[63] Betz O, Wegst U, Weide D, Heethoff M, Helfen L, Lee W-K, et al. Imaging applications of synchrotron X-ray phase-contrast microtomography in biological morphology and biomaterials science. I. General aspects of the technique and its advantages in the analysis of millimetre-sized arthropod structure. J Microsc 2007;227:51–71.
[64] Denk W, Horstmann H. Serial block-face scanning electron microscopy to reconstruct three-dimensional tissue nanostructure. PLoS Biol 2004;2:e329.
[65] Lipke E, Hörnschemeyer T, Pakzad A, Booth CR, Michalik P. Serial block-face imaging and its potential for reconstructing diminutive cell systems: a case study from arthropods. Microsc Microanal 2014:1–10.
[66] Harada S, Honda W, Arie T, Akita S, Takei K. Fully printed, highly sensitive multifunctional artificial electronic whisker arrays integrated with strain and temperature sensors. ACS Nano 2014;8:3921–7.
[67] Takei K, Yu Z, Zheng M, Ota H, Takahashi T, Javey A. Highly sensitive electronic whiskers based on patterned carbon nanotube and silver nanoparticle composite films. Proc Natl Acad Sci 2014. 201317920.
[68] Scholz GR, Rahn CD. Profile sensing with an actuated whisker. IEEE Trans Rob Autom 2004;20:124–7.
[69] Assaf T, Conn A, Rossiter J, Walters P, Pearson M. Artificial vibrissae DEA-based module. In: SPIE smart structures and materials + nondestructive evaluation and health monitoring: international society for optics and photonics; 2014. p. 90562O-O-9.
[70] Maravall M, Diamond ME. Algorithms of whisker-mediated touch perception. Curr Opin Neurobiol 2014;25:176–86.
[71] Diamond ME, Arabzadeh E. Whisker sensory system–from receptor to decision. Prog Neurobiol 2013;103:28–40.
[72] Fu J, Joshi SB, Catchmark JM. A study of angular effects in focused ion beam milling of water ice. J Micromech Microeng 2008;18:095010.
[73] Chan YL, Ngan AHW, King NM. Use of focused ion beam milling for investigating the mechanical properties of biological tissues: a study of human primary molars. J Mech Behav Biomed Mater 2009;2:375–83.
[74] Schertel A, Snaidero N, Han H-M, Ruhwedel T, Laue M, Grabenbauer M, et al. Cryo FIB-SEM: volume imaging of cellular ultrastructure in native frozen specimens. J Struct Biol 2013;184:355–60.